ACS SENSORS

pubs.acs.org/acssensors Article

Multifunctional Wearable System for Mapping Body Temperature and Analyzing Sweat

Md. Sajjad Alam, Jung Kyung Kim, and Jungil Choi*

Cite This: *ACS Sens.* 2023, 8, 1980−1988 Read Online

ACCESS | Metrics & More | Article Recommendations | Supporting Information

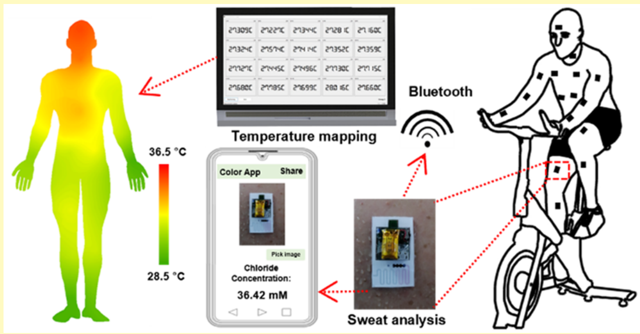

ABSTRACT: Integrated wearable bioelectronic health monitoring systems have revealed new possibilities for collecting personalized physiological information. Wearable sweat sensors have the potential to noninvasively measure valuable biomarkers. Mapping sweat and skin-temperature throughout the body can provide detailed information on the human body. However, existing wearable systems cannot evaluate such data. Here, we report a multifunctional wearable platform that can wirelessly measure local sweat loss, sweat chloride concentration, and skin temperature. The approach combines a reusable electronics module to monitor skin temperature and a microfluidic module for monitoring sweat loss and sweat chloride concentration. The miniaturized electronic system takes temperature measurements from the skin and wirelessly transmits the obtained data to a user device using Bluetooth technology. In contrast, the microfluidic system provides accurate colorimetric analysis of the chloride concentration and sweat loss. Thus, this integrated wearable system has great application potential in individualized health management systems for sports researchers and competitors and can also be applied in clinical settings.

KEYWORDS: *sweat, microfluidics, colorimetric, temperature mapping, wireless communication*

Nowadays, the design and advancement of wearable bioelectronic devices capable of real-time monitoring of physiological and biochemical signals have attracted significant attention. Wearable physical sensors facilitate wireless monitoring of several physiological parameters such as blood pressure,[1] heart rate,[2] and temperature.[3] Temperature is an important physiological parameter as it effects almost all human body activities related to metabolism.[4] A stable body temperature is crucial to maintain proper metabolism in the human body as hyperthermia or hypothermia adversely affects the enzymes responsible for metabolism.[5] Moreover, skin temperature provides information regarding skin injuries and diseases.[6]

In contrast, wearable chemical sensors offer noninvasive simultaneous monitoring of several crucial analytes in human biofluids, such as sweat,[7] saliva,[8] and interstitial fluid,[9] instead of invasive blood. Due to its ease of access and lack of invasiveness, sweat has gained greater attention than other biofluids in recent years. Human sweat secreted by eccrine glands is an analyte-rich fluid. Sweat contains several crucial biomarkers such as electrolytes (Cl^-, Na^+, and K^+), metabolites (urea, lactate, glucose, and ammonia), nutrients (Ca^{2+}, Mg^{2+}, vitamin c, and iron), toxins (ethanol), and hormones (cytokines and cortisol).[10] Sweat lactate provides information about physical stress and can be used to detect pressure ischemia.[11] Recent studies suggest that sweat glucose qualitatively indicates blood glucose levels and can thus be used for simultaneous monitoring of diabetes.[12] Sweat chloride concentration is a standard marker to test genetic conditions such as cystic fibrosis (CF) in newborns.[13] In addition, sweat rate indicates hydration state, physical exertion, and stress.[14]

Generally, sweat and temperature mapping studies are performed in a clinical laboratory environment that requires benchtop instruments. Conventional methodologies for sweat collection are related to use of wicking gauzes, centrifuge systems, and absorbent pads. However, these techniques cover only a small region of the body and do not offer real time sweat information. Moreover, these approaches suffer from contamination, and loss of samples during several analysis steps. Recent advances in microfluidic,[15] electrochemical,[16] and electronic[17] platforms have overcome these limitations by enabling real time analysis of sweat utilizing wireless near-field communication (NFC) or Bluetooth Low Energy (BLE) technologies. Traditionally, skin thermography utilizes an infrared (IR) digital camera system; however, it requires an expensive system. Recently developed skin-interfaced wearable temperature sensors enable continuous monitoring of skin temperature.[18]

Received: January 16, 2023
Accepted: April 13, 2023
Published: April 25, 2023

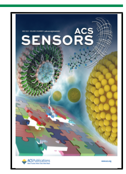

https://doi.org/10.1021/acssensors.3c00098
ACS Sens. 2023, 8, 1980−1988

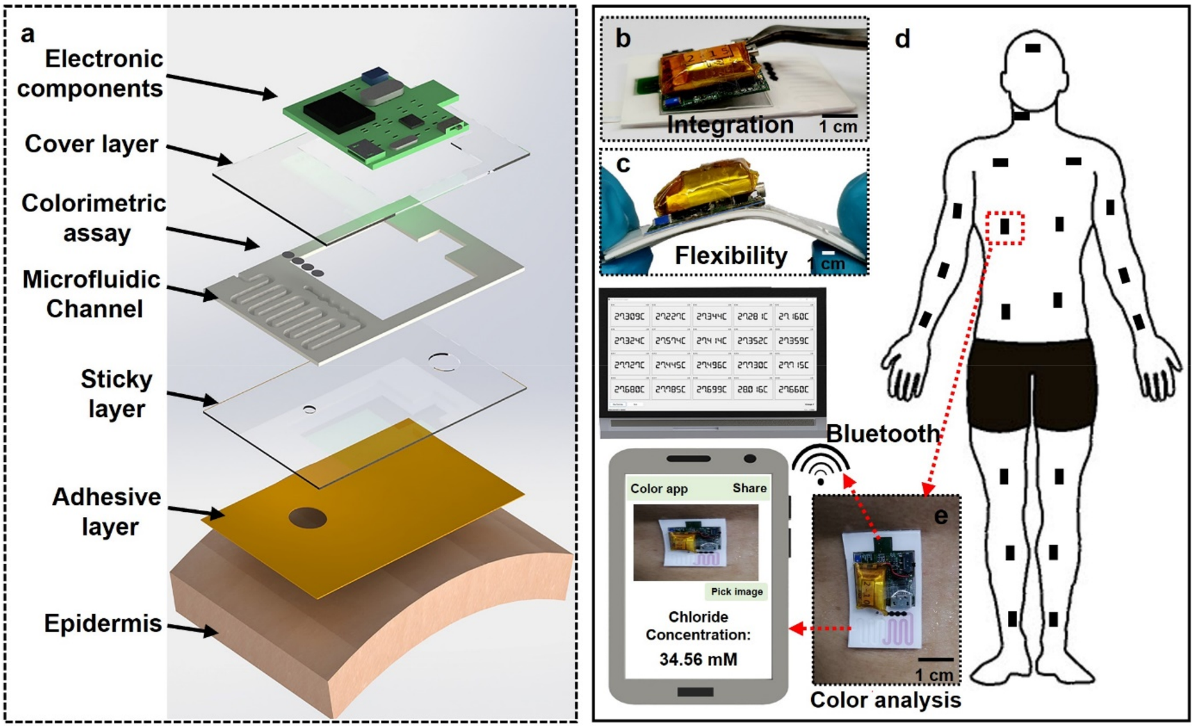

Figure 1. Schematic illustrations and photographs of wireless epidermal sensors used for monitoring body temperature and sweat. (a) Exploded view of schematic illustration of multifunctional sweat and temperature sensing platform. (b) Optical image of the system showing integration of microfluidic and electronic module. (c) Optical image of the complete system under bending condition. (d) Illustration of the epidermal sensors connected throughout the body with simultaneous, wireless data transmission capabilities. (e) Image of complete sensor attached to human skin during sweating.

Monitoring the sweat loss, sweat chloride, and temperature is essential to have a total understanding of the physiological health condition. For instance, mapping sweat chloride concentration throughout the body can help identify the CF, a genetic disorder that affects the lungs, pancreas, and other organs. Since a patient with this disease generally has 60−150 mM chloride concentration in sweat, for diagnosis of CF mapping chloride concentration is necessary to identify the severity and distribution of the disease.[19,20] In addition, monitoring sweat chloride concentration can help assess the effectiveness of treatment. By tracking changes in sweat chloride concentration over time, doctors can adjust medication dosages and other therapies to optimize outcome. Mapping the local sweat rate across the body is important while monitoring patients who have suffered from a stroke.[21] Furthermore, mapping the temperature throughout the body during sleep is useful to investigate the circadian rhythm sleep-wake disorders.[22] By mapping skin temperature over time, healthcare providers can monitor the infection and inflammation status of a wound.[23,24] Mapping sweat rate and sweat chloride concentration can provide information about the body's fluid and electrolyte imbalance, while mapping skin temperature can provide information about body's thermoregulatory process. Together, these parameters can provide a comprehensive assessment of individual's hydration status, which can be useful to prevent hyponatremia.[25,26]

Usually, full body sweat rate is determined by calculating the change in body weight before and after physical exercise. However, these methods need to consider several parameters such as food/water intake throughout the exercise period and are not useful in real-world cases. The existing sweat sensors mainly focus on individual monitoring of targeted analytes. In contrast, the existing temperature sensors mostly focus on body temperature measurement for a small area. However, monitoring sweat and skin temperature together can provide vital information about the human body. To the best of our knowledge, no effort has been made for mapping sweat and skin temperature throughout the body. Such monitoring requires integration of wearable chemical and physical sensors that can transfer data wirelessly.

Here, we introduce a multi-skilled wearable system for monitoring sweat loss, chloride concentration, and skin temperature. The system integrates physical and chemical sensors. The physical sensor utilizes an electronic module to measure skin temperature, and the chemical sensor utilizes a microfluidic module for sweat analysis. A custom developed smartphone application evaluates the sweat chloride concentration. Moreover, the system can measure skin temperature in a wireless manner for 10 h. A custom computer program is also developed to monitor these data in a single screen. This integration offers a facile way to monitor temperature and sweat for personalized healthcare systems.

■ MATERIALS AND METHODS

Fabrication of the Microfluidic Module. The microfluidic channels were fabricated using standard soft photolithography techniques. More precisely, a 200 μm SUEX TDFS photoresist (DJ Microlaminates, USA) was coated on a 500 μm thick, 4 in. silicon wafer at 70 °C. Afterward, the SUEX-coated silicon substrate was subjected to ultraviolet (UV) light at a power of 200 mJ m^{-2} through a predesigned photomask. Following photolithography, the coated silicon substrate was baked at 90 °C for 20 min on a pre- heated hot plate. After that, the silicon wafer was developed for 10 min utilizing an SU-8 developer (Kayaku Advanced Materials, USA). The polydimethylsiloxane (PDMS) base, curing agent (Sylgard 184, Dow Corning), and white silicone dye (Silc Pig, Smooth-On) were then mixed in a 10:1:1 weight ratio and put in a vacuum chamber for 15 min to remove generated air bubbles. Then, the degassed PDMS mixture was spin-coated on the developed mold at 200 rpm for 30 s, followed by baking at 140 °C for 3 min, to form the desired channel thickness. Following this, the channel layer was cut into the device size using a CO_2 laser cutter (Universal Laser Systems, USA). Pouring PDMS (10:1, base: curing agent) on a poly(methyl methacrylate) (PMMA)-treated silicon wafer and then spin-coating at 200 rpm for 30 s with subsequent curing at 140 °C for 3 min produced a 400-μm-thick uniform transparent cover layer. Later, the cover layer was cut into the temperature sensor block size. To create a sticky layer, we first prepared a 200-μm-thick PDMS layer (spin-coating at 400 rpm) on a PMMA-treated silicon wafer utilizing the procedure described above. On top of this, another layer of PDMS (40:1 base: curing agent ratio) was spin-coated at 1000 rpm for 30 s; the structure was cured at 140 °C for 3 min. The cover and sticky layers were bonded to the PDMS channel layer using a plasma treatment machine (BD-20 V, Electro-Technic Products, USA). A medical-grade adhesive layer was bonded to the back of the sticky layer after exposure to the plasma treatment machine. The detailed assembly of the system is included in the (SI) Supporting Information (Figure S1).

Fabrication of the Wireless Electronics Module. The electronic module consists of a microcontroller, an RF antenna, a USB connector, a Li-ion polymer battery, a low-dropout voltage regulator, a battery charge controller, a light-emitting diode, a digital temperature sensor, and passive components. A digital temperature sensor (MAX30208, Maxim Integrated, USA) with ±0.1 °C accuracy from +30 to +50 °C and 16-bit resolution (0.005 °C) detected the skin temperature of the human body. It utilized the standard interintegrated circuit (I^2C) serial communication bus to communicate with a microcontroller. The microcontroller block used a STM32WB55RGV6 (STMicroelectronics, Switzerland) chip, which is a low-power platform with Bluetooth 5 support. The chip transferred the temperature values to a computer program via the BLE protocol utilizing an RF antenna (ANT3216 LL00R2400A). A Li-ion polymer battery (TW601015-60 mAh) was used to power the system. The battery was charged with a linear charge management controller (MCP73830LT) and could be fully charged within 2 h. The battery could supply sufficient power to the system to simultaneously transmit temperature data for approximately 10 h. The circuit was designed in the OrCAD 9.2 capture platform. Afterward, a printed circuit board (PCB) layout was designed utilizing the PADS 9.4 layout platform. Subsequently, a four-layer PCB (area: 25 mm × 25 mm) that contained all the essential components for the electronics module was manufactured. The circuit diagram, routing at difference layers, PCB outline, and list of components are available in the Supporting Information (SI) (Figures S2−S4 and Table S1).

To monitor the temperature sensor data, a desktop application was developed using the C programming language in Microsoft Visual Studio 2017 development environment. The application displays the data of the 20 sensors simultaneously and allows the user to export the temperature data into a file in the comma-separated value (CSV) format. The materials and methods are provided in the SI.

■ RESULTS AND DISCUSSION

Multifunctional, Skin-Interfaced, Wearable System for Sweat Analysis and Temperature Mapping. An exploded view of the proposed hybrid sweat and temperature sensor is illustrated in Figure 1a. The prepared system is an integration of a microfluidic module for analyzing local sweat loss and chloride concentration and an electronics module for sensing skin temperature.

The dimension and weight of the device are 26 mm × 45 mm and 4.8 g (microfluidic module 1.7 g, electronics module 3.1 g), respectively. The microfluidic module is for single-time use, whereas the electronics module is reusable. The electronics module contains a wireless temperature sensor platform. A hole is created on the cover layer to attach the temperature sensor block on the bottom sticky layer. A chloride colorimetric assay is placed on the microchamber of microfluidic channel layer to detect the sweat chloride concentration. Moreover, a 5 mm-diameter hole on the bottom sticky layer allows the temperature sensor to remain in contact with the skin via adhesive layer for measuring skin temperature. A double-sided adhesive layer lies between the back of the sticky layer and epidermis, which offers comfortable attachment of the whole system on the skin. In our device, the temperature sensor is not in direct contact with the skin and if it did, it would measure the temperature of sweat on the skin rather than the skin temperature itself. Hence, we utilized the medical adhesive layer between the skin and the temperature sensor to ensure accurate skin-temperature measurement, as it provides good thermal contact without any air gaps that could affect the temperature reading.

Figure 1b demonstrates the integration of the microfluidic and electronics modules. The electronics module is attached through the hole of the cover layer to the bottom sticky layer. Figure 1c illustrates the flexibility of the system under bending conditions. The microfluidic module is flexible, whereas the temperature module is inflexible. However, the miniaturized temperature sensor in combination with the microfluidic module offers sufficient flexibility to attach the system on different curved regions of the human body. Figure 1d shows schematic of the sensors attached across the body, with wireless data transmission capabilities. Twenty devices were attached to different regions of the human body. The temperature sensors measure the skin temperature and transmit the data utilizing Bluetooth technology to a host computer. A custom computer application is developed to demonstrate the 20 temperature sensor values on a single screen.

During exercise, the body produces sweat to regulate its temperature by releasing heat from the body through the process of evaporation. This can potentially affect the accuracy of skin-temperature measurements, depending on various factors such as physical activity, sweat production, and sensor location. As our temperature sensor contacted to skin via the adhesive layer and covered by several PDMS layers, the evaporative cooling effect is not feasible for our device. The generated sweat enters the microfluidic channel via an inlet hole, and it fills the microchamber containing the colorimetric assay system. The amount of obtained color and chloride concentration are proportionate to each other. A color analysis smartphone application detects the chloride concentration based on the generated color values. The system does not require any color reference marker as it use the substrate to compensate the color in different lighting conditions. Moreover, the system facilitates quantitative monitoring of regional sweat loss. The amount of sweat in the microfluidic channel represents the local sweat loss. Figure 1e shows a complete photograph of the proposed hybrid system attached to the human skin during sweating.

Fundamental Characteristics of Wireless Temperature Sensor. Thermocouples, heat flux, and IR thermometry are commonly used skin-temperature sensors. Thermocouples generate a voltage proportional to the temperature difference between the two ends of the sensor when exposed to a temperature change. Heat flux sensor measures the flow of heat by detecting the temperature difference between two points on the surface being measured. IR thermometers measure temperature by detecting the infrared radiation emitted by an object. Among them we choose max30208 temperature sensor as it has small size, and suitable for wearable application. It utilizes an

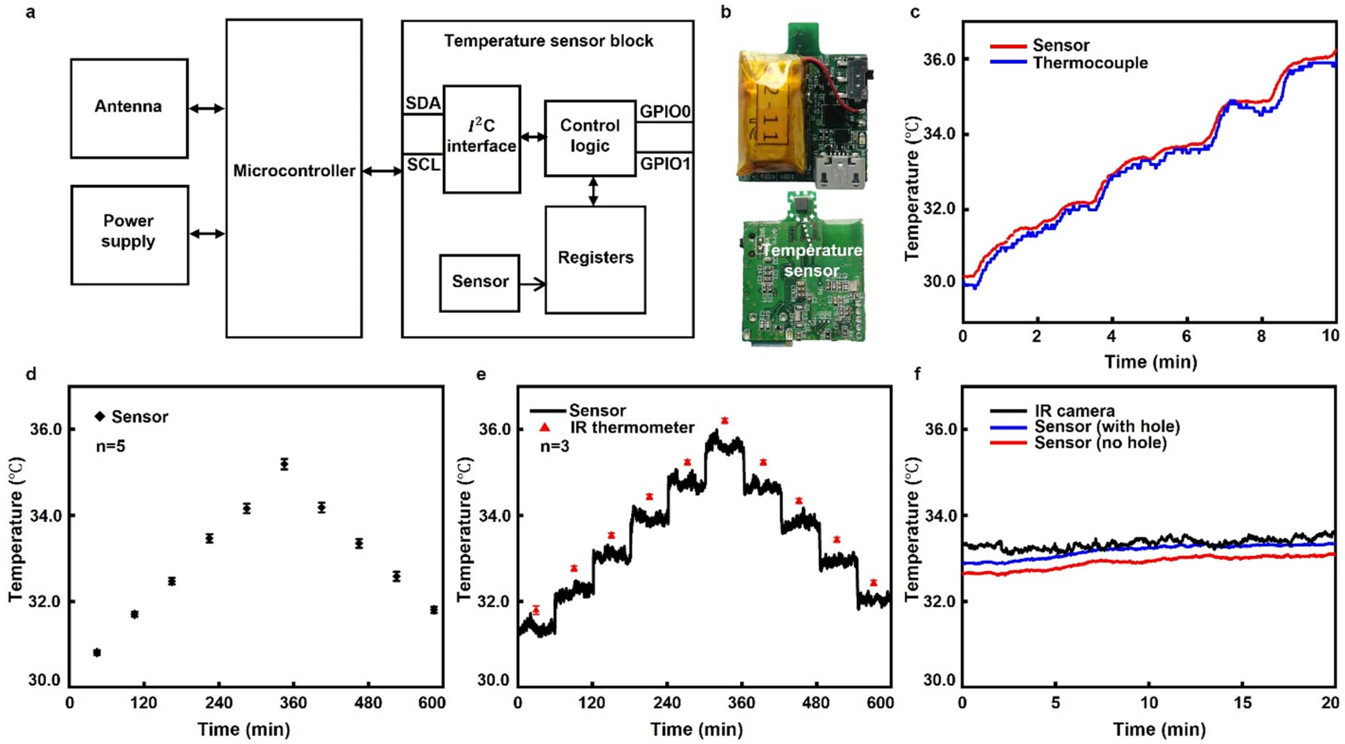

Figure 2. Wireless system for simultaneous measurement of body temperature. (a) Block diagram of temperature sensing platform. (b) Photograph of the complete temperature sensing system. (c) Comparison of the temperature sensor with a commercial thermocouple from 30 to 36 °C. (d) Calibration graph between time and temperature for five different temperature sensors. (e) Continuous 10 h performance comparison with that of an IR thermometer. (f) Comparison between the IR camera and temperature sensors with and without a hole in the adhesive layer.

integrated thermistor, and the thermistor's resistance changes with temperature.

The basic characteristics of the temperature sensors are investigated by evaluating the performance, calibration, long-term stability, and different environmental condition tests. The temperature sensor performance is compared with a commercial T-type thermocouple, and a commercial IR camera. Furthermore, the long-term stability test investigates the reliability of the temperature sensor in a 10 h test period. Figure 2a shows the block diagram of the proposed temperature sensor platform. The construction includes a temperature sensor, a microcontroller, an antenna, and a power supply for the system. A contact-based digital temperature sensor measured the skin temperature with 1 Hz sampling rate and utilized I^2C to communicate with a microcontroller. The microcontroller transfers the data to a host device using Bluetooth. Figure 2b shows photographs of the front and back view of the overall temperature sensor platform.

Figure 2c compares the performance of the temperature sensor with a commercial thermocouple from 30 to 36 °C. Notably, there is small difference (around 0.2 °C) in between the thermocouple and temperature sensor measurements. The experimental configuration is in the SI (Figure S5). Figure 2d shows the calibration graph between time and temperature for five different temperature sensors. It is noticeable that there is small difference between the five sensors measurement in 10 h period. Figure 2e displays the continuous 10-h performance results of the temperature sensor. The result indicates that the temperature sensor is reliable for 10 h measurement. In addition, we performed a 10 h comparison between the sensors and a thermocouple to assess the sensor's reliability further, which is in the SI (Figure S6).

Figure 2f compares the performance of the two sensors with an IR camera. Two sensors, one with a hole in the adhesive layer and another without hole were prepared and attached to the forearm of the human body. Afterward, an IR camera was used to monitor the forearm temperature. The sensor with a hole has direct contact with the skin, whereas the sensor without a hole is attached to the skin through an adhesive layer. The sensor with a hole measured a higher temperature compared to that without a hole. Moreover, some discrepancy is noticeable between the IR camera and temperature sensor results. This might be attributed to the different measurement techniques and effect of surrounding environment on the IR camera readings. The experimental setup is depicted in the SI (Figure S7). If the temperature sensor is exposed to sweat, it may affect the measurement of skin temperature. Therefore, we used an adhesive layer to block physical contact between the sweat and the temperature sensor throughout the experiment.

Besides, we investigated the effect of environmental condition on our device. We attached two devices on the left forearm and exposed them to different conditions, including a laboratory environment at 16 °C and 26% humidity, an outdoor environment at 4 °C and 23% humidity, a laboratory environment again at 16 °C and 27% humidity, and a warm room at 29 °C and 18% humidity. We also used a Fluke 62 MAX + (Fluke Corp, USA) IR thermometer to measure skin temperature and a Braun ThermoScan 7 (Braun, Germany) ear thermometer to measure core temperature using the left ear. We found that core body temperature decreased slightly in a cooler environment and that the skin temperature of the exposed forearm area was more affected by the surrounding environment compared to the unexposed sensor area. The

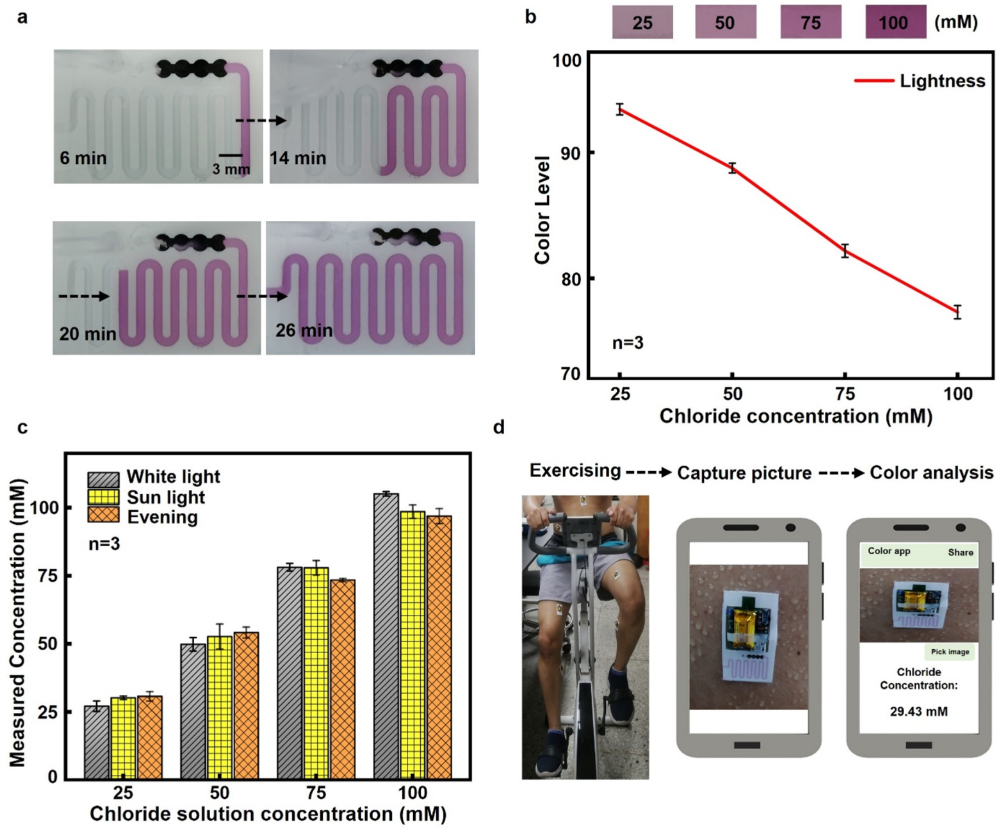

Figure 3. Skin-interfaced microfluidic platform for analyzing sweat. (a) Optical images of the microfluidic sweat sensor filling with time. (b) Optical image of colorimetric assay for sweat chloride detection. (c) Validation of the color reference marker at different lighting conditions (white light, sunlight, evening light) utilizing smartphone application. (d) Whole procedure of collecting and analyzing sweat chloride concentration.

experimental setup and results are presented in the SI (Figure S8).

Microfluidic Channel for Measuring Sweat Chloride Concentration and Local Sweat Loss. The microfluidic channel allows measurement of the sweat chloride concentration and local sweat loss. The width and depth of the microfluidic channel are 1 mm and 200 μm, respectively. Figure 3a illustrates an optical image of the microfluidic sensor filled with NaCl solution using a syringe infusion pump (KdScientific, Legato 200) at a volumetric rate of 1 μL/min. Notably, the first column of the microfluidic channel was filled in 6 min, and it took approximately 26 min to fill the entire microfluidic channel. Figure 3b demonstrates the colorimetric assay of chloride developed to evaluate the standard color of chloride at known concentration. A microfluidic system for chloride detection was prepared by drop-casting a 4 μL mixture comprising 200 μL of 2% polyhydroxyethyl methacrylate (pHEMA) and 50 mg of silver chloranilate into a microfluidic chamber. When sweat enters via the inlet and passes through the microchamber, it reacts with the silver chloranilate and produces purple color. The generated color density is proportional to the chloride concentration in sweat. An image processing algorithm was used to develop the color analysis software. The technique includes capturing images of the microfluidic channel, selection of region of interest, and comparison of color with predefined standard colors. The algorithm allowed facile conversion from typical RGB (red, green, blue) color space to CIE LAB color-space, which represents color in lightness (L), green to red color (a), and blue to yellow color (b). The algorithm used the hue-independent parameter lightness, which was later compared with the known lightness values. Sweat chloride concentration evaluation process using the smartphone application is demonstrated in the SI (Figure S9).

Figure 3c shows color reference marker at various ambient lighting conditions. To eliminate the difference in lighting conditions, the algorithm uses the white PDMS substrate as a reference color marker. However, around 5 mM uncertainties were found for variable lighting conditions. Figure 3d shows the overall procedure of sweat collection and analysis of color values utilizing the smartphone application. By taking pictures at each time point, we can monitor changes over time. Continuous measurement of chloride levels is not feasible with our current colorimetric method, as it necessitates manual measurements. An alternative solution is to incorporate an ion-selective electrochemical sensor into the system for continuous measurements.

The local sweat loss was determined utilizing the microfluidic channel. The exercise continued until sweat filled one microfluidic device fully. Later, we captured images of microfluidic channel to determine the filled volume of the channel via AutoCAD 2022 software. The total volume of a filled microfluidic channel is 26.5 μL, and the filled volume represents the local sweat loss for that region. The sweat loss evaluation at different bending condition is presented in the SI (Figure S10).

Full Body Temperature Mapping by Wearable Temperature Sensors. We measured the skin temperature during sleeping and daily life activities to explore the mapping capabilities of the temperature sensor. Figure 4a illustrates the measured body temperature during the 10-h daily life monitoring study. We observed a relatively stable core body

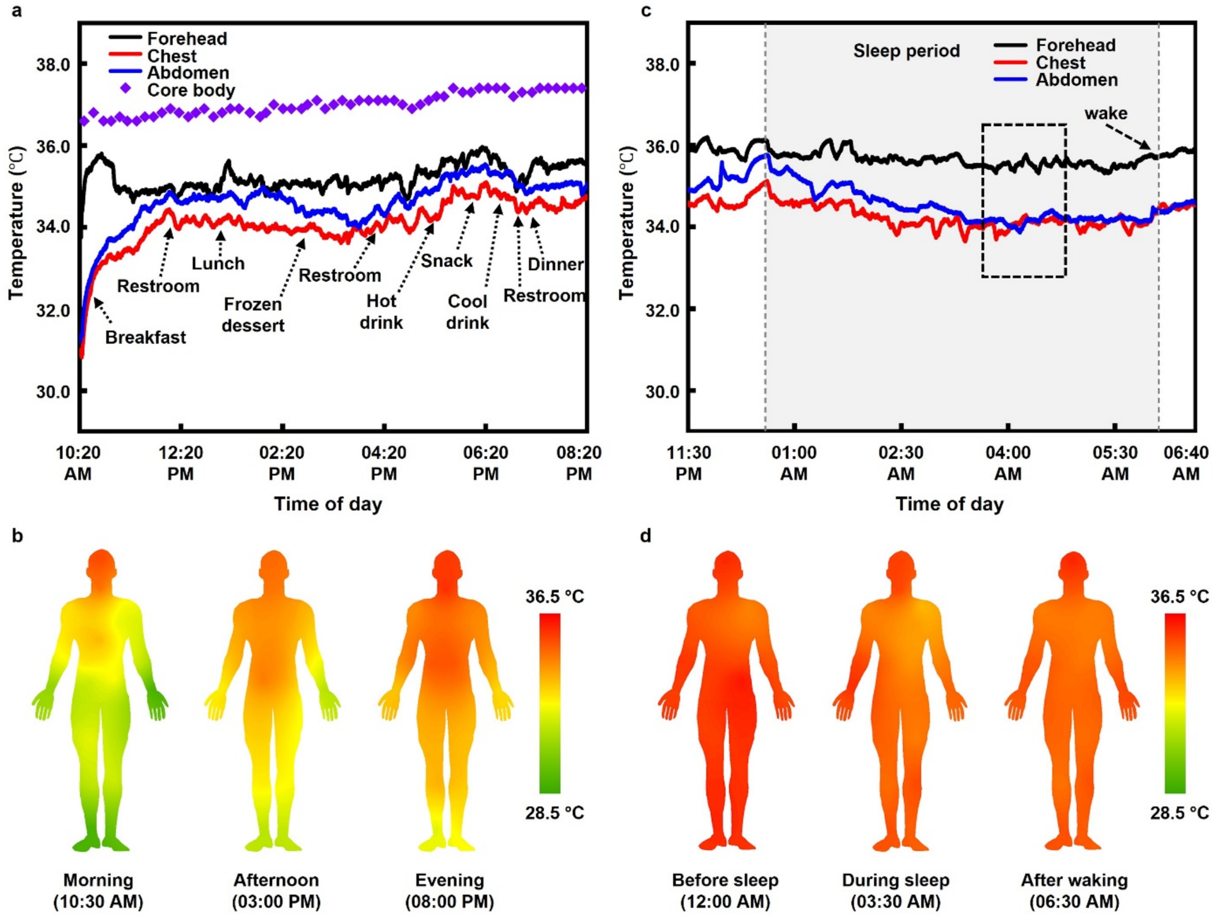

Figure 4. Wireless whole body temperature mapping. (a) Graphical illustration of skin temperature during daily life activities. (b) Color maps of skin temperature during the morning, afternoon, and evening in the study period. (c) Graphs of skin temperature at different body regions during the sleep study period. (d) Color mapping of temperature throughout the body regions before sleep, during sleep, and after awaking.

temperature over the course of study. We measured temperature using a Braun ThermoScan 7 ear thermometer and took measurements at 10 min intervals from the left ear. We found that core body temperature decreased by 0.1 °C immediately after breakfast but increased by 0.1 °C after lunch and dinner. After 30 min, the temperature remained unchanged. In contrast, skin temperature in the forehead, chest, and abdomen regions increased by an average of 0.16, 0.04, and 0.26 °C immediate after breakfast, lunch, and dinner, respectively. After 30 min, it increased by 0.31 and 0.14 °C for breakfast and dinner, respectively, but remained relatively stable for lunch. The slight increment in temperature observed after meals is due to an increase in metabolic rate.[27]

The consumption of cool drinks resulted in a 0.2 °C decrease in core body temperature 15 min after ingestion, due to the body expending energy to heat the cool water to its optimal temperature. Meanwhile, the forehead and abdomen skin temperature decreased by 0.31 and 0.12 °C, respectively, while chest temperature remained relatively stable. The study involved the consumption of 500 mL of iced water with a temperature of 1.1 °C. Consuming cold water can trigger body's thermoregulatory mechanisms to reduce blood flow to the skin and increase heat production, resulting in a drop in core body temperature.[28] Furthermore, it is though that absorption rate of cold water is slower compared to warm water, which may lead to decrease in skin temperature.[29]

In contrast, consumption of 500 mL of a hot drink such as milk at 57.5 °C results in a 0.2 °C increase in core body temperature 15 min after consumption, along with a corresponding rise in skin temperature in the forehead, chest, and abdomen regions by 0.34, 0.39, and 0.17 °C, respectively. The increase in core and skin temperature suggests that the body increased its metabolic rate and blood flow to the skin to dissipate excess heat generated by the hot drink.[30,31] Additionally, we observed that consuming frozen desserts like ice cream led to a slight reduction in both core and skin temperature, while eating snacks such as cookies resulted in a minor elevation in core and skin temperature.

Figure 4b demonstrates the color mapping of body temperature during the morning, afternoon, and evening periods. It is noticeable from Figure 4b that the overall body temperature increases from morning to evening. The measured temperature data for 10 h in the daily life monitoring study are available in the SI (Figure S11). Figure 4c presents the graphical illustration of body temperature during the 7 h sleep study. The sleep study period is indicated by the gray boundary. The body temperature decreases from the beginning of sleep and reaches a minimum value 2 h prior to waking, which is similar to the results reported earlier.[32,33] The dashed-border rectangle box represents the minimum body temperature regions during sleep. The average body temperature of the forehead, chest, and abdomen regions experienced a decrement of 0.87 °C during the sleep period. Figure 4d shows the heat color map of the entire body

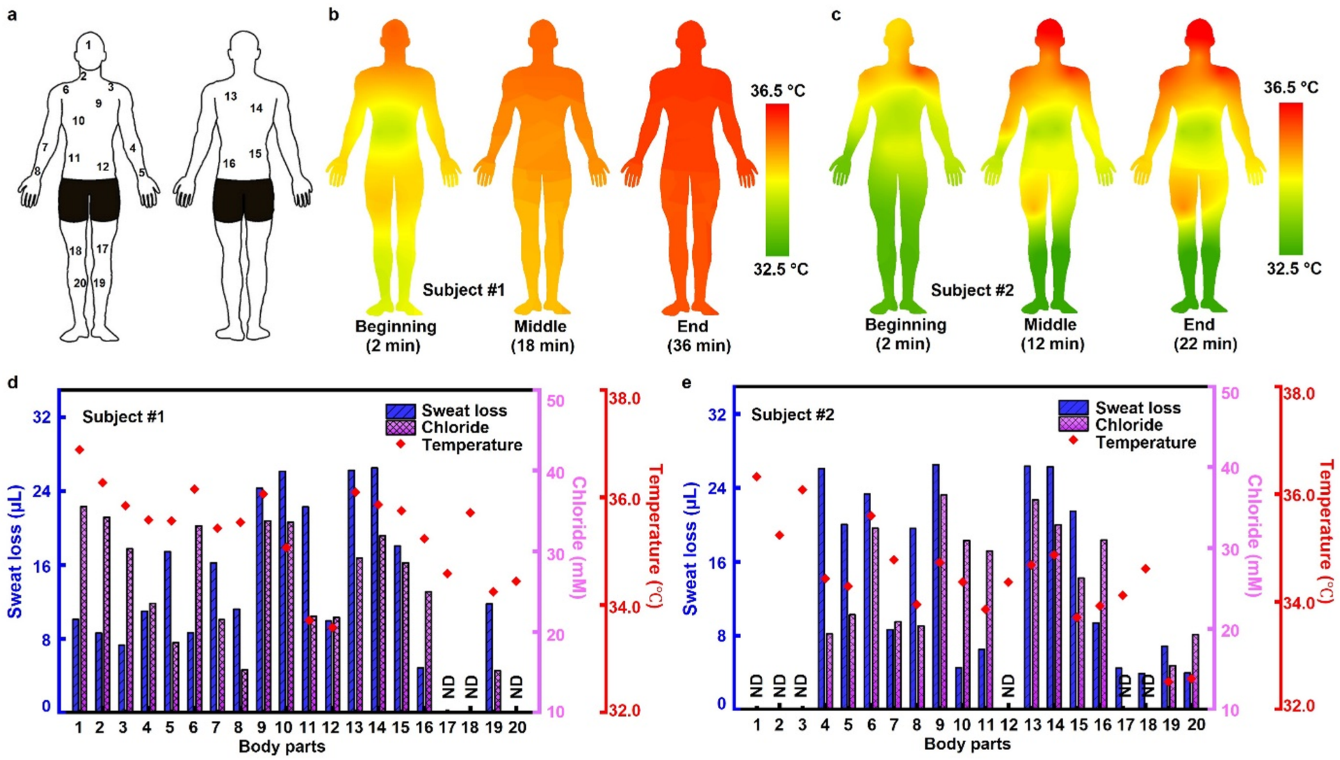

Figure 5. Mapping sweat and body temperature during exercise. (a) Diagram of placement of 20 sensors on the front and back of the human body. (b) Color map of skin temperature (subject #1). (c) Color map of skin temperature (subject #2). (d) Graphical demonstration of skin temperature, sweat loss, and chloride concentration (subject #1). (e) Graphical representation of sweat loss, chloride concentration, and skin temperature (subject #2).

temperature just before sleep, during sleep, and soon after waking. Notably, the core region of the body has higher temperature than the peripheral regions. Although the body temperature decreased during sleep, it started to increase after waking. The 7 h sleep-study data is situated in the SI (Figure S12).

Full Body Sweat and Temperature Mapping during Physical Exercise. To explore the versatility of the proposed system, a physical exercise test was conducted, where two volunteers were riding a stationary bike, and the corresponding skin temperature was monitored wirelessly. The sweat loss and chloride concentration values were also determined by employing the color values. The proposed sensors were used to obtain a single measurement of the chloride concentration, which represented the average value over the entire experiment. The load of the stationary bike was kept constant as an increment, or a decrement of load resulted in a change in sweat chloride concentration.[34] Figure 5a illustrates a schematic diagram of the 20 sensors located at the front and back of the body for the physical exercise study. The body area is divided in different section and relatively flat surface was chosen for better attachment of sensors. Figure 5b and c demonstrates the heat color map at the beginning, middle, and end of exercise for subject #1 and subject #2 respectively. The color maps were generated utilizing only the temperature sensors located on the front side of the body. It is noticeable that for both cases at the beginning (2 min of exercise), the body temperature is lower than those in the middle and end of the exercise period.

Figure 5d shows the graphical illustration of the overall sweat and temperature profile for subject #1. It is noticeable that the head, chest, and back regions have a higher sweat chloride concentration than other regions of the body, which is consistent with the earlier reported findings.[35,36] For instance, the maximum chloride concentration was determined on the forehead region, i.e., 35.54 mM (#1 device). Moreover, the average chloride concentrations calculated for the chest and back regions were 33.66 and 28.65 mM, respectively. In contrast, the measured chloride concentration on the forearm region was 22.54 mM. The sweat losses from the head, chest, and back regions were found to be higher than those from other regions. The maximum amount of sweat loss was calculated from the upper back (#14 device) region, i.e., 26.51 μL. In addition, the average sweat losses from the chest and forehead regions were 25.24 and 10.11 μL, respectively. In contrast, the average sweat losses from the forearm and leg regions were 13.62 and 11.8 μL, respectively. The temperature profile in Figure 5d shows the average temperature values throughout the exercise period. Notably, the head, chest, and back regions have a higher temperature than the other regions. The full body temperature results for subject #1 is available in the SI (Figure S13).

Figure 5e shows the overall sweat and temperature profile for subject #2. It is noteworthy that the chest and back regions have a higher sweat loss and chloride concentration than those of other regions. For instance, the maximum sweat loss and chloride concentration were found for the chest (#9 device), i.e., 26.51 μL and 36.58 mM, respectively. In contrast, the average sweat loss and chloride concentration from the forearm region were determined to be 17.375 μL and 20.12 mM, respectively. The average temperature profile in Figure 5e shows the high temperature of the head, chest, and back regions of the body. Therefore, we can conclude that, in most cases, higher sweat losses lead to a higher sweat chloride concentration. Furthermore, generally higher sweat chloride concentration leads to a higher skin temperature.

https://doi.org/10.1021/acssensors.3c00098
ACS Sens. 2023, 8, 1980−1988

For both subjects #1 and #2, the amounts of sweat in the leg regions were lower. Due to insufficient sweat generation, the sweat profile was not determined for some regions (denoted as "ND"). The entire body temperature data for subject#2 can be found in the SI (Figure S14).

CONCLUSION

We proposed and demonstrated a skin-compatible, multidisciplinary wearable wireless platform for monitoring sweat loss and chloride concentration together with skin temperature. This technique integrates a reusable electronics module and a microfluidic module. The electronic system exploits a miniaturized PCB technology that includes a precise temperature sensor and a microcontroller with Bluetooth functionality for wireless transfer of skin-temperature data. The microfluidic module utilizes the colorimetric approach to monitor chloride concentration. The set of 20 Bluetooth based skin-temperature sensors can map the body temperature in daily life, sleep, and exercise conditions. At the same time, the microfluidic sweat sensor measures local sweat loss and sweat chloride concentration. From the various tests performed in the lab and on the body, the integrated device showed its capability to study body temperature and sweating.

ASSOCIATED CONTENT

Supporting Information

The Supporting Information is available free of charge at https://pubs.acs.org/doi/10.1021/acssensors.3c00098.

Materials and Methods; Step-by-step assembly of the system; Circuit diagram of the electronics module; Electronics module PCB routing; PCB outline of the electronics module; Temperature sensor performance comparison with a thermocouple; Temperature sensor's reliability test; Adhesive layer effect evaluation process; Device performance evaluation under various environmental conditions; Sweat loss evaluation at different bending condition; Sweat chloride concentration evaluation process using smartphone application; Daily life monitoring results obtained with wireless temperature sensors; Sleep study results obtained with wireless temperature sensors; Measurements of skin temperature during physical exercise (subject#1); Results of skin temperature during physical exercise (subject#2); List of components used in the PCB of electronics module (PDF)

Firmware and software components: Custom-developed firmware for Microcontroller, Bluetooth, and Color analysis application (ZIP)

AUTHOR INFORMATION

Corresponding Author

Jungil Choi – *Department of Mechanical Engineering, Ajou University, Suwon 16499, Republic of Korea;* orcid.org/0000-0002-3659-8978; Email: cji@ajou.ac.kr

Authors

Md. Sajjad Alam – *Department of Mechanical Engineering, Kookmin University, Seoul 02707, Republic of Korea*

Jung Kyung Kim – *School of Mechanical Engineering and Department of Integrative Biomedical Science and Engineering, Kookmin University, Seoul 02707, Republic of Korea;* orcid.org/0000-0002-4164-6655

Complete contact information is available at: https://pubs.acs.org/10.1021/acssensors.3c00098

Author Contributions

Md. Sajjad Alam: Conceptualization, Methodology, Software, Formal analysis, Investigation, Data curation, Writing–original draft, Visualization, Writing–review and editing. **Jung Kyung Kim:** Supervision, Conceptualization, Visualization, Validation, Writing–review and editing. **Jungil Choi:** Supervision, Conceptualization, Methodology, Software, Validation, Funding acquisition, Data curation, Visualization, Writing–review and editing.

Notes

The authors declare no competing financial interest.

ACKNOWLEDGMENTS

This work was supported by the National Research Foundation of Korea (NRF) grant funded by the Korean Government (Grant No. 2022R1C1C1010059) and the support from the new faculty research fund of Ajou University.

REFERENCES

(1) Schwartz, G.; Tee, B. C. K.; Mei, J.; Appleton, A. L.; Kim, D. H.; Wang, H.; Bao, Z. Flexible Polymer Transistors with High Pressure Sensitivity for Application in Electronic Skin and Health Monitoring. *Nat. Commun.* **2013**, *4* (May), 1859.

(2) Hong, Y. J.; Lee, H.; Kim, J.; Lee, M.; Choi, H. J.; Hyeon, T.; Kim, D. H. Multifunctional Wearable System That Integrates Sweat-Based Sensing and Vital-Sign Monitoring to Estimate Pre-/Post-Exercise Glucose Levels. *Adv. Funct. Mater.* **2018**, *28* (47), 1805754.

(3) Wu, Z.; Ding, H.; Tao, K.; Wei, Y.; Gui, X.; Shi, W.; Xie, X.; Wu, J. Ultrasensitive, Stretchable, and Fast-Response Temperature Sensors Based on Hydrogel Films for Wearable Applications. *ACS Appl. Mater. Interfaces* **2021**, *13* (18), 21854–21864.

(4) Kuht, J.; Farmery, A. D. Body Temperature and Its Regulation. *Anaesth. Intensive Care Med.* **2018**, *19* (9), 507–512.

(5) Khan, Y.; Ostfeld, A. E.; Lochner, C. M.; Pierre, A.; Arias, A. C. Monitoring of Vital Signs with Flexible and Wearable Medical Devices. *Adv. Mater.* **2016**, *28* (22), 4373–4395.

(6) Webb, R. C.; Bonifas, A. P.; Behnaz, A.; Zhang, Y.; Yu, K. J.; Cheng, H.; Shi, M.; Bian, Z.; Liu, Z.; Kim, Y. S.; Yeo, W. H.; Park, J. S.; Song, J.; Li, Y.; Huang, Y.; Gorbach, A. M.; Rogers, J. A. Ultrathin Conformal Devices for Precise and Continuous Thermal Characterization of Human Skin. *Nat. Mater.* **2013**, *12* (10), 938–944.

(7) Caldara, M.; Colleoni, C.; Guido, E.; Re, V.; Rosace, G. Optical Monitoring of Sweat PH by a Textile Fabric Wearable Sensor Based on Covalently Bonded Litmus-3-Glycidoxypropyltrimethoxysilane Coating. *Sensors Actuators, B Chem.* **2016**, *222*, 213–220.

(8) Kim, J.; Imani, S.; de Araujo, W. R.; Warchall, J.; Valdés-Ramírez, G.; Paixão, T. R. L. C.; Mercier, P. P.; Wang, J. Wearable Salivary Uric Acid Mouthguard Biosensor with Integrated Wireless Electronics. *Biosens. Bioelectron.* **2015**, *74*, 1061–1068.

(9) Tierney, M. J.; Tamada, J. A.; Potts, R. O.; Jovanovic, L.; Garg, S. Clinical Evaluation of the GlucoWatch Biographer: A Continual, Non-Invasive Glucose Monitor for Patients with Diabetes. *Biosens. Bioelectron.* **2001**, *16* (9–12), 621–629.

(10) Baker, L. B.; Wolfe, A. S. *Physiological Mechanisms Determining Eccrine Sweat Composition*; Springer: Berlin, Heidelberg, 2020; Vol. *120*.

(11) Derbyshire, P. J.; Barr, H.; Davis, F.; Higson, S. P. J. Lactate in Human Sweat: A Critical Review of Research to the Present Day. *J. Physiol. Sci.* **2012**, *62* (6), 429–440.

(12) Moyer, J.; Wilson, D.; Finkelshtein, I.; Wong, B.; Potts, R. Correlation between Sweat Glucose and Blood Glucose in Subjects with Diabetes. *Diabetes Technol. Ther.* **2012**, *14* (5), 398–402.

(13) Farrell, P. M.; Rosenstein, B. J.; White, T. B.; Accurso, F. J.; Castellani, C.; Cutting, G. R.; Durie, P. R.; LeGrys, V. A.; Massie, J.;

Parad, R. B.; Rock, M. J.; Campbell, P. W. Guidelines for Diagnosis of Cystic Fibrosis in Newborns through Older Adults: Cystic Fibrosis Foundation Consensus Report. *J. Pediatr.* **2008**, *153* (2), S4.

(14) Baker, L. B. Sweating Rate and Sweat Sodium Concentration in Athletes: A Review of Methodology and Intra/Interindividual Variability. *Sport. Med.* **2017**, *47*, 111−128.

(15) Choi, J.; Bandodkar, A. J.; Reeder, J. T.; Ray, T. R.; Turnquist, A.; Kim, S. B.; Nyberg, N.; Hourlier-Fargette, A.; Model, J. B.; Aranyosi, A. J.; Xu, S.; Ghaffari, R.; Rogers, J. A. Soft, Skin-Integrated Multifunctional Microfluidic Systems for Accurate Colorimetric Analysis of Sweat Biomarkers and Temperature. *ACS Sensors* **2019**, *4* (2), 379−388.

(16) Bandodkar, A. J.; Gutruf, P.; Choi, J.; Lee, K. H.; Sekine, Y.; Reeder, J. T.; Jeang, W. J.; Aranyosi, A. J.; Lee, S. P.; Model, J. B.; Ghaffari, R.; Su, C. J.; Leshock, J. P.; Ray, T.; Verrillo, A.; Thomas, K.; Krishnamurthi, V.; Han, S.; Kim, J.; Krishnan, S.; Hang, T.; Rogers, J. A. Battery-Free, Skin-Interfaced Microfluidic/Electronic Systems for Simultaneous Electrochemical, Colorimetric, and Volumetric Analysis of Sweat. *Sci. Adv.* **2019**, *5* (1), 1−16.

(17) Gao, W.; Emaminejad, S.; Nyein, H. Y. Y.; Challa, S.; Chen, K.; Peck, A.; Fahad, H. M.; Ota, H.; Shiraki, H.; Kiriya, D.; Lien, D. H.; Brooks, G. A.; Davis, R. W.; Javey, A. Fully Integrated Wearable Sensor Arrays for Multiplexed in Situ Perspiration Analysis. *Nature* **2016**, *529* (7587), 509−514.

(18) Webb, R. C.; Bonifas, A. P.; Behnaz, A.; Zhang, Y.; Yu, K. J.; Cheng, H.; Shi, M.; Bian, Z.; Liu, Z.; Kim, Y. S.; Yeo, W. H.; Park, J. S.; Song, J.; Li, Y.; Huang, Y.; Gorbach, A. M.; Rogers, J. A. Ultrathin Conformal Devices for Precise and Continuous Thermal Characterization of Human Skin. *Nat. Mater.* **2013**, *12* (10), 938−944.

(19) LeGrys, V. A.; Yankaskas, J. R.; Quittell, L. M.; Marshall, B. C.; Mogayzel, P. J. Diagnostic Sweat Testing: The Cystic Fibrosis Foundation Guidelines. *J. Pediatr.* **2007**, *151* (1), 85−89.

(20) Rock, M. J.; Makholm, L.; Eickhoff, J. A New Method of Sweat Testing: The CF Quantum sweat Test. *J. Cyst. Fibros.* **2014**, *13* (5), 520−527.

(21) Korpelainen, J. T.; Sotaniemi, K. A.; Myllylä, V. V. Hyperhidrosis as a Reflection of Autonomic Failure in Patients with Acute Hemispheral Brain Infarction: An Evaporimetric Study. *Stroke* **1992**, *23* (9), 1271−1275.

(22) Abbott, S. M.; Reid, K. J.; Zee, P. C. Circadian Rhythm Sleep-Wake Disorders. *Psychiatr. Clin. North Am.* **2015**, *38* (4), 805−823.

(23) Lou, D.; Pang, Q.; Pei, X.; Dong, S.; Li, S.; Tan, W. q.; Ma, L. Flexible Wound Healing System for Pro-Regeneration, Temperature Monitoring and Infection Early Warning. *Biosens. Bioelectron.* **2020**, *162* (February), 112275.

(24) Hattori, Y.; Falgout, L.; Lee, W.; Jung, S. Y.; Poon, E.; Lee, J. W.; Na, I.; Geisler, A.; Sadhwani, D.; Zhang, Y.; Su, Y.; Wang, X.; Liu, Z.; Xia, J.; Cheng, H.; Webb, R. C.; Bonifas, A. P.; Won, P.; Jeong, J. W.; Jang, K. I.; Song, Y. M.; Nardone, B.; Nodzenski, M.; Fan, J. A.; Huang, Y.; West, D. P.; Paller, A. S.; Alam, M.; Yeo, W. H.; Rogers, J. A. Multifunctional Skin-like Electronics for Quantitative, Clinical Monitoring of Cutaneous Wound Healing. *Adv. Healthc. Mater.* **2014**, *3* (10), 1597−1607.

(25) Heikenfeld, J. Non-Invasive Analyte Access and Sensing through Eccrine Sweat: Challenges and Outlook circa 2016. *Electroanalysis* **2016**, *28* (6), 1242−1249.

(26) Coury, A. J.; Fogt, E. J.; Norenberg, M. S.; Untereker, D. F. Development of a Screening System for Cystic Fibrosis. *Clin. Chem.* **1983**, *29* (9), 1593−1597.

(27) Rowe, B. G. G.; Maxwell, G. M.; Castillo, C. A.; Freeman, D. J.; Crumpton, C. W. A STUDY IN MAN OF CEREBRAL BLOOD FLOW AND CEREBRAL GLUCOSE, LACTATE AND PYRUVATE METABOLISM BEFORE AND AFTER EATING. *J. Clin. Invest.* **1959**, *38*, 2154−2158.

(28) Lu, C. C.; Li, M. H.; Lin, T. C.; Chen, T. L.; Chen, R. M.; Tung, C. S.; Tseng, C. J.; Ho, S. T. Water Ingestion Reduces Skin Blood Flow through Sympathetic Vasoconstriction. *Clin. Auton. Res.* **2012**, *22* (2), 63−69.

(29) Mori, Y.; Miwa, C.; Maeda, K.; Hamaguchi, H.; Mizutani, M.; Deguchi, A.; Shimasaki, H. Effects of Temperature of Drinking Water on Regulation of Body Temperature in Humans. *J. Japanese Soc. Balneol. Climatol. Phys. Med.* **2019**, *82* (2), 78−85.

(30) Lee, J. K. W.; Shirreffs, S. M. The Influence of Drink Temperature on Thermoregulatory Responses during Prolonged Exercise in a Moderate Environment. *J. Sports Sci.* **2007**, *25* (9), 975−985.

(31) Lee, J. K. W.; Maughan, R. J.; Shirreffs, S. M. The Influence of Serial Feeding of Drinks at Different Temperatures on Thermoregulatory Responses during Cycling. *J. Sports Sci.* **2008**, *26* (6), 583−590.

(32) Okawa, M.; Uchiyama, M. Circadian Rhythm Sleep Disorders: Characteristics and Entrainment Pathology in Delayed Sleep Phase and Non-24 Sleep-Wake Syndrome. *Sleep Med. Rev.* **2007**, *11* (6), 485−496.

(33) Han, S.; Kim, J.; Won, S. M.; Ma, Y.; Kang, D.; Xie, Z.; Lee, K. T.; Chung, H. U.; Banks, A.; Min, S.; Heo, S. Y.; Davies, C. R.; Lee, J. W.; Lee, C. H.; Kim, B. H.; Li, K.; Zhou, Y.; Wei, C.; Feng, X.; Huang, Y.; Rogers, J. A. Battery-Free, Wireless Sensors for Full-Body Pressure and Temperature Mapping. *Sci. Transl. Med.* **2018**, *10* (435), eaan4950.

(34) Choi, D. H.; Kitchen, G. B.; Stewart, K. J.; Searson, P. C. The Dynamic Response of Sweat Chloride to Changes in Exercise Load Measured by a Wearable Sweat Sensor. *Sci. Rep.* **2020**, *10* (1), 1−10.

(35) Taylor, N. A. S.; Machado-Moreira, C. A. Regional Variations in Transepidermal Water Loss, Eccrine Sweat Gland Density, Sweat Secretion Rates and Electrolyte Composition in Resting and Exercising Humans. *Extrem. Physiol. Med.* **2013**, *2*, 4.

(36) Sonner, Z.; Wilder, E.; Heikenfeld, J.; Kasting, G.; Beyette, F.; Swaile, D.; Sherman, F.; Joyce, J.; Hagen, J.; Kelley-Loughnane, N.; Naik, R. The Microfluidics of the Eccrine Sweat Gland, Including Biomarker Partitioning, Transport, and Biosensing Implications. *Biomicrofluidics* **2015**, *9* (3), 031301.

https://doi.org/10.1021/acssensors.3c00098
ACS Sens. 2023, 8, 1980−1988